University of Massachusetts Amherst

ScholarWorks@UMass Amherst

Mathematics and Statistics Department Faculty Publication Series

Mathematics and Statistics

2009

Spinor Bose-Einstein condensates in double-well potentials

C Wang

PG Kevrekidis
University of Massachusetts - Amherst, kevrekid@math.umass.edu

N Whitaker

TJ Alexander

DJ Frantzeskakis

See next page for additional authors

Follow this and additional works at: https://scholarworks.umass.edu/math_faculty_pubs

Part of the Physical Sciences and Mathematics Commons

Recommended Citation

Authors
C Wang, PG Kevrekidis, N Whitaker, TJ Alexander, DJ Frantzeskakis, and P Schmelcher

Spinor Bose-Einstein condensates in double well potentials

C. Wang[1], P.G. Kevrekidis[1], N. Whitaker[1],
T.J. Alexander[2], D.J. Frantzeskakis[3] and P. Schmelcher[4,5]

[1] Department of Mathematics and Statistics, University of Massachusetts,
Amherst MA 01003-4515, USA

[2] Nonlinear Physics Center, Research School of Physical Sciences
and Engineering, Australian National University, Canberra ACT 0200, Australia

[3] Department of Physics, University of Athens, Panepistimiopolis,
Zografos, Athens 157 84, Greece

[4] Theoretische Chemie, Institut für Physikalische Chemie, Im Neuenheimer Feld 229,
Universität Heidelberg, 69120 Heidelberg, Germany

[5] Physikalisches Institut, Philosophenweg 12, Universität Heidelberg
69120 Heidelberg, Germany

November 13, 2008

Abstract

We consider the statics and dynamics of $F = 1$ spinor Bose-Einstein condensates (BECs) confined in double well potentials. We use a two-mode Galerkin-type quasi-analytical approximation to describe the stationary states of the system. This way, we are able to obtain not only earlier results based on the *single mode approximation* (SMA) frequently used in studies of spinor BECs, but also additional modes that involve either two or all three spinor components of the $F = 1$ spinor BEC. The results based on this Galerkin-type decomposition are in good agreement with the analysis of the full system. We subsequently analyze the stability of these multi-component states, as well as their dynamics when we find them to be unstable. The instabilities of the symmetric or anti-symmetric states exhibit symmetry-breaking and recurrent asymmetric patterns. Our results yield qualitatively similar bifurcation diagrams both for polar (such as ^{23}Na) and ferromagnetic (such as ^{87}Rb) spinor BECs.

1 Introduction

In the past few years, there has been a remarkable amount of progress in the study of Bose-Einstein condensates (BECs) [1, 2] and an intense investigation of the localized nonlinear states that can be formed therein [3]. From the nonlinear dynamics point of view, one of the features that makes this system a particularly relevant and interesting one is associated with the presence of a diverse range of external potentials which are used to trap the atoms magnetically, optically or electrically (or

through combinations thereof) [1, 2, 3]. Hence, monitoring the existence, stability and dynamical properties of nonlinear localized modes within these diverse potentials has become a principal theme of research effort, especially within the realm of the prototypical mean-field model, namely the Gross-Pitaevskii (GP) equation (which is a variant of the nonlinear Schrödinger (NLS) equation extensively used in nonlinear optics [4]).

While most of the work in BECs has centered around one-component systems, more recently far-off-resonant optical techniques for trapping ultracold atomic gases [5], have produced an intense focus on the study of *spinor* BECs [6, 7], in which the spin degree of freedom (frozen in magnetic traps) emerges. In this context, various phenomena absent in single-component BECs may arise in the dynamical evolution of multi-component spinor condensates [8], including the formation of spin domains [9] and spin textures [10], spin-mixing dynamics [11], dynamic fragmentation [12], or dynamics of quantum phases [13]. Moreover, macroscopic nonlinear states in the form of multi-component vector solitons of the bright [14, 15, 16], dark [17] and gap [18] type, along with more complex structures, such as bright-dark soliton complexes [19] and domain walls [20], have also been studied.

On the other hand, as indicated above, one of the most attractive traits of such ultracold systems is the possibility of experimental realization of different potentials. Among them, one that has drawn considerable attention due to its fundamental nature is the double-well potential. One of the prototypical realizations thereof comes from combining a strong harmonic trap with a periodic lattice [21]. In this context, the study of BECs loaded in double well potentials allows for the investigation of a variety of fundamental phenomena, including Josephson oscillations and tunneling for a small number of atoms, or macroscopic quantum self-trapping and an asymmetric partition of the atoms between the wells for sufficiently large numbers of atoms [21]. Double well potentials have also spurred numerous theoretical insights including, among others, finite-mode reductions, analytical results for specially designed shapes of the potential and quantum depletion effects [22, 23, 24, 25, 26, 27, 28, 29, 30]. It should be noted that such potentials have also been studied in the context of nonlinear optics, with relevant experimental results appearing, e.g., in twin-core self-guided laser beams in Kerr media [31] and optically induced dual-core waveguiding structures in photorefractive crystals [32].

The principal scope of the present work is to combine these two interesting developments, namely to examine spinor BECs in the presence of double well potentials. In particular, our aim is to present a systematic classification of the states that are possible for $F = 1$ spinor condensates confined in a double well potential. This classification is formulated on the basis of a two-mode Galerkin-type approximation of the stationary states of the system, which involves the decomposition of the spatial part of the solutions into a linear combination of the eigenfunctions of the underlying linear operator; the relevant two-mode reduction used here is in the spirit of Galerkin truncations in finite element and similar methods (see, e.g., Ref. [33]). Such an approach can provide a detailed analytical handle on the dynamics of this multi-component BEC system (see, e.g., the earlier work on one-component [29] and two-component BECs [34] in double well potentials). It should be noted here that such attempts have been made before, most notably in Refs. [35] and [36]: the first of these works examined magnetization oscillations and beats among other dynamical states, while the second one (which provided a description beyond mean-field theory) examined quantum entanglement and pseudo-spin-squeezing properties. However, these works were constrained within

the commonly used *single mode approximation* (SMA) for spinor condensates (see, e.g., [11, 37, 38]) in which the wavefunction of each of the three components is taken to be a time-dependent multiple of a single stationary state. One of the particularly interesting features in the present setting is that the two-mode Galerkin-type approximation reveals a considerable wealth of states, many of which can not be described in the framework of SMA. In particular, as we will see below, there is a multitude of states which are symmetric in some of the components, while they are anti-symmetric in others, and out of these states also bifurcate further states which are asymmetric (but often in a non-single-mode way) in the different components. Many of these novel states have a good chance to be observed in experiments with quasi one-dimensional (1D) spinor BECs since, by performing their linear stability analysis, we find them to be stable. Finally, we examine the dynamical evolution of both two-component and three-component states that we find to be unstable; we observe that the manifestation of the associated instabilities is exhibited typically through symmetry-breaking between the components and is also associated with recurring asymmetric patterns.

The paper is structured as follows. In section 2, we present the model, and provide the analytical approach. In section 3, we present our numerical results. In particular, we obtain the complete bifurcation diagram of the possible stationary states, both for the full three-component system, as well as for the two-mode Galerkin-type approximation (in very good agreement between the two). In that section, we also illustrate the spatial profiles of the nonlinear modes arising in the spinor condensate and quantify their stability. Lastly, we corroborate these stability predictions by performing dynamical simulations of the unstable modes. Finally, in section 4, we summarize our findings and present our conclusions, as well as some topics for future study.

2 The model and the analytical approach

In the framework of mean-field theory, the wavefunctions $\psi_{\pm 1,0}(x,t)$ of the three hyperfine components ($m_F = \pm 1, 0$) of a quasi-1D spinor $F = 1$ condensate is governed by the following system of coupled normalized GP equations [18]:

$$i\partial_t \psi_{\pm 1} = \mathcal{L}\psi_{\pm 1} + \nu_s S \psi_{\pm 1} + \nu_a (S - 2|\psi_{\mp 1}|^2)\psi_{\pm 1} + \nu_a \psi_0^2 \psi_{\mp 1}^* \qquad (2.1)$$

$$i\partial_t \psi_0 = \mathcal{L}\psi_0 + \nu_s S \psi_0 + \nu_a (S - |\psi_0|^2)\psi_0 + 2\nu_a \psi_0^* \psi_1 \psi_{-1}. \qquad (2.2)$$

In these expressions $S = |\psi_{-1}|^2 + |\psi_0|^2 + |\psi_1|^2$ represents the total normalized density, while the coupling coefficients ν_s and ν_a represent, respectively, the symmetric spin-independent and the antisymmetric spin-dependent interaction strengths (see, e.g., [18] for details). Additionally,

$$\mathcal{L}\psi_j = -\frac{1}{2}\partial_x^2 \psi_j + V(x)\psi_j, \qquad (2.3)$$

($j = -1, 0, 1$) represents the single-particle operator with a confining potential $V(x)$ assumed to be of the form

$$V(x) = \frac{1}{2}\Omega^2 x^2 + V_0 \text{sech}^2(x/w). \qquad (2.4)$$

This is a double well potential consisting of a parabolic potential of strength Ω emulating, e.g., a usual harmonic trap, and a localized barrier potential of strength V_0 and width w, representing, e.g., a blue-detuned laser beam that repels atoms from the harmonic trap center. Notice that the main

qualitative features of our results (i.e., the nature of the bifurcation diagram near the linear limit, the emergence of the symmetry-breaking asymmetric states, and their dynamical manifestations) do not rely on the specific form of the double well potential and should be expected to arise more broadly within this class of models (spinor condensates in double well potentials).

We now seek stationary solutions of Eqs. (2.1)-(2.2) in the form $\psi_j = u_j \exp(-i\mu_j t)\exp(i\theta_j)$, where μ_j and θ_j correspond, respectively, to the chemical potentials and phases of the wavefunctions obeying the usual constraints (see, e.g., [37, 20]), namely, $2\mu_0 = \mu_1 + \mu_{-1}$ and $\Delta\theta = 2\theta_0 - (\theta_1 + \theta_{-1}) = 0$ or π. These are the so-called phase matching conditions relevant for stationary states typically in systems with parametric interactions; see, e.g., Ref. [39] for the case of four-wave mixing in nonlinear optics. This ansatz results in the following equations for the stationary states u_j:

$$\mu_{\pm 1} u_{\pm 1} = \mathcal{L}u_{\pm 1} + \nu_s S u_{\pm 1} + \nu_a(S - 2u_{\mp 1}^2)u_{\pm 1} \pm \nu_a u_0^2 u_{\mp 1}, \tag{2.5}$$

$$\mu_0 u_0 = \mathcal{L}u_0 + \nu_s S u_0 + \nu_a(S - u_0^2)u_0 \pm 2\nu_a u_0 u_1 u_{-1}, \tag{2.6}$$

where the $\pm$ sign in the last terms of the above equations corresponds, respectively, to the cases of $\Delta\theta = 0$ and $\Delta\theta = \pi$.

The basic idea of the two mode Galerkin-type approximation [23, 26, 28, 29] that we will employ to approximate the solutions of Eqs. (2.5)-(2.6) is the following: we assume that in the vicinity of the linear limit of the system (and for appropriate selection of the chemical potential) each of the states $u_{\pm 1,0}$ can be decomposed into a two-mode expansion, involving the symmetric ground state and the antisymmetric first excited state of the underlying linear potential. We will denote those states by ϕ_a and ϕ_b, respectively, and accordingly decompose u_j (where $j \in \{-1, 0, 1\}$) as follows,

$$u_j(x,t) = c_a^{(j)}\phi_a(x) + c_b^{(j)}\phi_b(x), \tag{2.7}$$

where $c_a^{(j)}$ and $c_b^{(j)}$ are unknown time-dependent complex prefactors. By substituting Eq. (2.7) into Eqs. (2.5)-(2.6), and upon projecting each of the three equations in (2.5)-(2.6) to ϕ_a and ϕ_b, we obtain through tedious but straightforward algebra, the following six nonlinear, *algebraic* equations describing the stationary states of the original system [1]

$$\begin{aligned}
\mu_{\pm 1}c_a^{(\pm 1)} &= \omega_a c_a^{(\pm 1)} + \nu_s\left[\Gamma_a S_a c_a^{(\pm 1)} + \Gamma_{ab}S_b c_a^{(\pm 1)} + \Gamma_{ab}S_{ab}c_b^{(\pm 1)}\right] \\
&+ \nu_a\left[\nu_a(S_a - 2(c_a^{(\mp 1)})^2)c_a^{\pm 1} + \Gamma_{ab}(S_b - 2(c_b^{(\mp 1)})^2)c_a^{(\pm 1)} + \Gamma_{ab}(S_{ab} - 4c_a^{(\mp 1)}c_b^{(\mp 1)})c_b^{(\pm 1)}\right] \\
&\pm \nu_a\left[\Gamma_a(c_a^{(0)})^2 c_a^{(\mp 1)} + \Gamma_{ab}(c_b^{(0)})^2 c_a^{(\mp 1)} + 2\Gamma_{ab}c_a^{(0)}c_b^{(0)}c_b^{(\mp 1)}\right], \tag{2.8}
\end{aligned}$$

$$\begin{aligned}
\mu_{\pm 1}c_b^{(\pm 1)} &= \omega_b c_b^{(\pm 1)} + \nu_s\left[\Gamma_b S_b c_b^{(\pm 1)} + \Gamma_{ab}S_a c_b^{(\pm 1)} + \Gamma_{ab}S_{ab}c_a^{(\pm 1)}\right] \\
&+ \nu_a\left[\Gamma_b(S_b - 2(c_b^{(\mp 1)})^2)c_b^{\pm 1} + \Gamma_{ab}(S_a - 2(c_a^{(\mp 1)})^2)c_b^{(\pm 1)} + \Gamma_{ab}(S_{ab} - 4c_a^{(\mp 1)}c_b^{(\mp 1)})c_a^{(\pm 1)}\right] \\
&\pm \nu_a\left[\Gamma_b(c_b^{(0)})^2 c_b^{(\mp 1)} + \Gamma_{ab}(c_a^{(0)})^2 c_b^{(\mp 1)} + 2\Gamma_{ab}c_a^{(0)}c_b^{(0)}c_a^{(\mp 1)}\right], \tag{2.9}
\end{aligned}$$

$$\begin{aligned}
\mu_0 c_a^{(0)} &= \omega_a c_a^{(0)} + \nu_s\left[\Gamma_a S_a c_a^{(0)} + \Gamma_{ab}S_b c_a^{(0)} + \Gamma_{ab}S_{ab}c_b^{(0)}\right] \\
&+ \nu_a\left[\Gamma_a(S_a - (c_a^{(0)})^2)c_a^{(0)} + \Gamma_{ab}(S_b - (c_b^{(0)})^2)c_a^{(0)} + \Gamma_{ab}(S_{ab} - 2c_a^{(0)}c_b^{(0)})c_b^{(0)}\right]
\end{aligned}$$

---

[1]Note that since we are interested in stationary states herein, we will consider $c_a^{(j)}$ and $c_b^{(j)}$ to be independent of time, although the expansion can also be used to probe the dynamics, by substituting the ansatz of Eq. (2.7) with time-dependent coefficients into Eqs. (2.1)-(2.2) and projecting into ϕ_a and ϕ_b.

$$\pm \quad 2\nu_a \left[\Gamma_a(c_a^{(0)})c_a^{(1)}c_a^{(-1)} + \Gamma_{ab}(c_a^{(0)})c_b^{(-1)}c_b^{(1)} + \Gamma_{ab}(c_a^{(-1)}c_b^{(1)} + c_b^{(-1)}c_a^{(1)})c_b^{(0)} \right], \quad (2.10)$$

$$\mu_0 c_b^{(0)} \quad = \quad \omega_b c_b^{(0)} + \nu_s \left[\Gamma_b S_b c_b^{(0)} + \Gamma_{ab} S_a c_b^{(0)} + \Gamma_{ab} S_{ab} c_a^{(0)} \right]$$

$$+ \quad \nu_a \left[\Gamma_b(S_b - (c_b^{(0)})^2)c_b^{(0)} + \Gamma_{ab}(S_a - (c_a^{(0)})^2)c_b^{(0)} + \Gamma_{ab}(S_{ab} - 2c_a^{(0)}c_b^{(0)})c_a^{(0)} \right]$$

$$\pm \quad 2\nu_a \left[\Gamma_b(c_b^{(0)})c_b^{(1)}c_b^{(-1)} + \Gamma_{ab}(c_b^{(0)})c_a^{(-1)}c_a^{(1)} + \Gamma_{ab}(c_a^{(-1)}c_b^{(1)} + c_b^{(-1)}c_a^{(1)})c_a^{(0)} \right]. \quad (2.11)$$

In these equations, $\omega_{a,b}$ are the eigenvalues that correspond to the linear eigenfunctions $\phi_{a,b}$, respectively, $S_a = \sum_j (c_a^{(j)})^2$, $S_b = \sum_j (c_b^{(j)})^2$, $S_{ab} = \sum_j 2c_a^{(j)}c_b^{(j)}$, while the coefficients $\Gamma_a = \int \phi_a^4 dx$, $\Gamma_b = \int \phi_b^4 dx$ and $\Gamma_{ab} = \int \phi_a^2 \phi_b^2 dx$ are constants that depend on the potential.

By solving this algebraic set of equations, for appropriate parameters of the potential [e.g., in the normalization detailed below (see Section 3) using the mean-field interaction energy, for $\Omega = 0.2$, $V_0 = 1$ and $w = 0.5$, $\omega_a = 0.249$, $\omega_b = 0.315$, and $\Gamma_a = 0.127$, $\Gamma_b = 0.134$ and $\Gamma_{ab} = 0.120$], we can extract all the potential stationary states for a given combination of chemical potentials in the two-parameter space (μ_0, μ_1) [recall that μ_{-1} is fully determined by the above two parameters]. Then, these can be used as initial guesses for identifying these solutions in the full nonlinear eigenvalue problem of Eqs. (2.5)-(2.6).

Some special cases of solutions can be found in the above algebraic equations. Since these have been discussed in earlier works in one-component systems (see, e.g., [29]), two-component systems (see, e.g., [34]), and even in the full three-component system but in the context of the SMA (see e.g., [11, 18, 37, 38]), we relegate the relevant detailed analysis of these to Appendix A. Importantly, we note that the principal building blocks of the single component setting are a symmetric state, where only c_a (of a particular component) is non-zero, an anti-symmetric state with only $c_b \neq 0$, as well as asymmetric states with both c_a and $c_b \neq 0$. The latter bifurcate beyond a critical point from the symmetric state if $\nu_s < 0$, or from the antisymmetric state if $\nu_s > 0$ [29].

In the next section, we will offer the full set of solutions that can be constructed within our two-mode Galerkin-type approximation and compare them to the detailed numerical results of the original problem.

3 Numerical Results

Before proceeding further, it is necessary to provide here values of the physical parameters that we will use. First we note that for simplicity in our computations we use the rescaling of ν_s to 1 and of ν_a to $\nu_a/\nu_s \equiv \delta$. Notice that in the relevant cases of the ferromagnetic ^{87}Rb and polar ^{23}Na spinor ($F = 1$) condensates, the parameter δ takes the values $\delta = -4.66 \times 10^{-3}$ [40] and $\delta = +3.14 \times 10^{-2}$ [41], respectively. Under this rescaling, the connection between physical values and dimensionless parameters is as described in detail in Refs. [19, 20]. We will also fix the double well potential parameters to the values $\Omega = 0.2$, $V_0 = 1$ and $w = 0.5$ (other values lead to qualitatively similar results). Taking into regard that the normalized chemical potentials will take values $\mu_j \approx 0.5$, this choice may correspond, e.g., to a spinor condensate of sodium atoms confined in a highly asymmetric trap with frequencies $\omega_\perp = 3\omega_x = 2\pi \times 230$ Hz, with peak 1D density $n_0 \simeq 10^8$ m^{-1} and number of atoms of order $O(10^3)$. In this case, the time and space units in the numerical results that will be presented below are 1.2 ms and 1.8 μm, respectively.
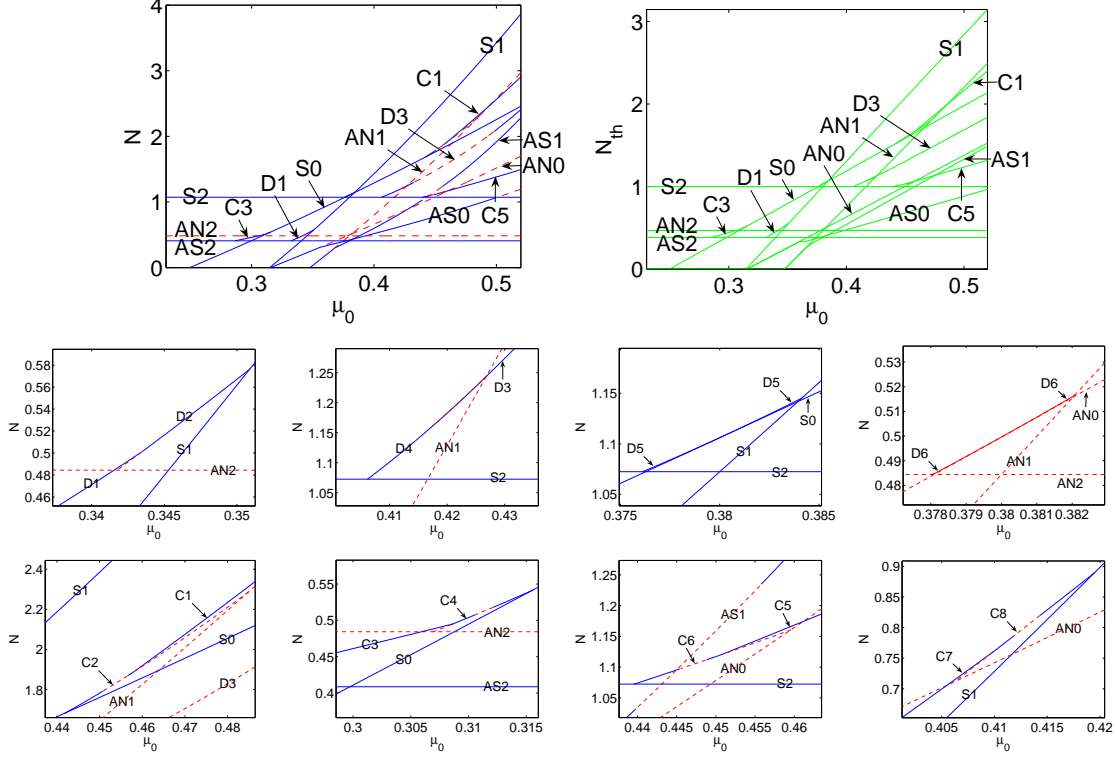
Figure 1: (Color online) Top panels: the norm N (normalized number of atoms) of the numerically found solutions of Eqs. (2.1)-(2.2) (left) and their counterparts predicted by the two-mode Galerkin-type approximation (right) for the case of the ^{23}Na spinor BEC, as a function of μ_0 with fixed $\mu_{-1} = 0.38$. Middle and bottom panels: blowups of segments in the top left panel where new combined solutions emerge at the relevant bifurcation points. All blowups, except the last one, are dedicated to the case of $\mu_{-1} = 0.38$ as in the top left panel. The last one, showing the branches C7 and C8 (see text) corresponds to the case of $\mu_{-1} = 0.48$ (as in the top left panel of Fig. 7 below). The branches D1 and D3 are generated from D2 and D4, respectively. Branches labeled by D (D1-D6 in the different panels of the figure) correspond to waveforms with two nonzero components, u_1 and u_{-1}; see the discussion of section 3.1 and Figs. 3 -4 for more details. The branches C1, C3, C5 and C7 are generated from C2, C4, C6 and C8, respectively. Branches labeled by C (C1-C8 in the different panels of the figure) correspond to waveforms with all three components nonzero; see the discussion of section 3.2 and Figs. 5-6 for more details. Solid (blue) lines and dashed (red) lines denote stable and unstable solutions, respectively.

Perhaps the cornerstone of the present work is encapsulated within Fig. 1, generated for the case of a ^{23}Na spinor condensate. This, admittedly, rather busy diagram encompasses *all* possible states near the linear limit of a spinor BEC loaded in a double well potential. Among them, one can discern one-component states that are well-known from the considerations of single-component double well settings [21, 22, 26, 29] for each one of the three components (labeled by S for symmetric, AN for antisymmetric and AS for asymmetric realizations of each component); see also Fig. 2. They are labeled by 1 when they belong to component u_1, by 0 when they belong to u_0 and by 2 when they belong to u_{-1}. Notice that the AS state bifurcates from the S state in the attractive case and from the AN state in the repulsive case, inheriting their stability (and rendering them unstable, through a pitchfork bifurcation) [29].

Importantly, the graph also contains two-component states involving components with subscripts 1 and -1 (and with a vanishing 0 component), denoted collectively by D and analyzed in Section 3.1 below (cf. also [34]). These are branches involving the symmetric and/or antisymmetric components of u_1 and u_{-1}; interestingly, out of these branches bifurcate new asymmetric solutions involving the same two components.

Finally, branches with contributions from all three components are also identified and are collectively labeled by C; these are examined more systematically in Section 3.2 below. These predominantly consist of either components u_1 and u_0 (with a small component in u_{-1}) or u_{-1} and u_0 (with a small component u_1). Again different combinations of symmetric and/or antisymmetric configurations are possible among these components, and additional asymmetric branches are observed to bifurcate from them. We now turn to a more detailed explanation of our findings.

To analyze the stability of a particular state (in this case and in the following ones), we perform linearization around the unperturbed state u_j, assuming a perturbed solution of Eqs. (2.1)-(2.2) in the form,

$$\psi_j = \exp(-i\mu_j t) \left[u_j + \epsilon \left(p_j(x) \exp(\lambda t) + q_j^\star(x) \exp(\lambda^\star t) \right) \right] \tag{3.1}$$

where p_j and q_j represent infinitesimal perturbations with eigenvalues $\lambda \equiv \lambda_r + i\lambda_i$ (here ϵ is a formal small parameter and the asterisk denotes complex conjugate). When its relevant eigenvalues are found to be purely imaginary, then the corresponding state is linearly stable, while the presence of eigenvalues with $\lambda_r \neq 0$ is tantamount to instability. Then, the results of the linear stability analysis are typically presented in the spectral plane (λ_r, λ_i). A typical example is provided in Fig. 2, where we show the profiles and the corresponding spectral planes (λ_r, λ_i) of the branches S1, AN1, and AS1.

Coming back to the bifurcation diagram of Fig. 1, it is important to highlight that it has been constructed by fixing μ_{-1} and varying only μ_1 and μ_0 (since one of these three quantities is always slaved to the variation of the other two). For this reason, S2, AN2 and AS2 are horizontal lines since μ_{-1} is fixed in the case studied below (i.e., their properties do not change as (μ_1, μ_0) are varied.) We will vary μ_0 while doing the analysis, with μ_1 being determined by $\mu_1 = 2\mu_0 - \mu_{-1}$.

3.1   Two-component states

In addition to "pure" branches populating only one component, there also exist additional branches populating two components, similarly to the results of Ref. [34]. In Fig. 1, prototypical examples of
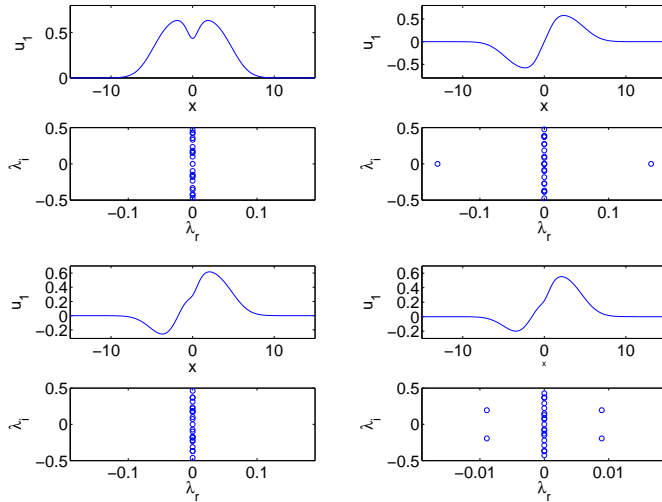
Figure 2: (Color online) Profiles of wave functions u_1 (first and third rows) and stability eigenvalues (second and fourth rows) corresponding to S1, AN1 and AS1 (branches of these solutions are shown in Fig. 1): S1 for $\mu_0 = 0.48$ (top left), AN1 for $\mu_0 = 0.48$ (top right), AS1 for $\mu_0 = 0.48$ (third row left) and AS1 for $\mu_0 = 0.45$ (third row right).

these branches are given by D1-D6 which involve the two components u_1 and u_{-1}. More specifically, D2 "connects" S1 and AN2. That is to say that D2 has a symmetric wavefunction in the component u_1, while it has an antisymmetric one in component u_{-1}. D1 bifurcates from D2, below a critical number of atoms through a pitchfork bifurcation, is asymmetric in both components u_1 and u_{-1} and eventually merges into AS2. It is relevant to point out here that in the first panel of the second row of Fig. 1, it appears as if D2 and D1 are essentially overlapping for the small fraction of the D2 branch for which they coexist (in this segment, D2 is unstable). However D2 terminates into AN2, while D1 continues to exist for lower norms, down to AS2. In a situation entirely similar to that highlighted above, but now between S2 and AN1, the branch that "connects" them is D4. Out of that branch with a symmetric wavefunction in u_{-1} and an anti-symmetric in u_1 bifurcates (above a critical norm N) the branch D3 which is again asymmetric in both of these components, and will eventually merge with AS1. Since these two situations (involving D1,D2 and D3,D4, respectively) are essentially similar (both of the bifurcation sub-structures are shown in Fig. 1), only the latter pair of branches is examined in detail in Fig. 3. In particular, it can be seen there that while the D4 branch is stable before D3 appears, the supercritical pitchfork leading to the emergence of D3 destabilizes D4. On the other hand, D3 itself may be unstable but only due to Hamiltonian-Hopf bifurcations [42], associated with weak complex quartets of eigenvalues. Finally, in terms of two-component branches, in addition to the above pairs connecting the symmetric nonlinear eigenmodes of one component with the anti-symmetric ones of the other, there also exist the branches D5 and D6 (see again the blowups of Fig. 1). These connect the symmetric state of u_1 (branch S1) with the symmetric state of u_{-1} (branch S2) and the antisymmetric state of u_1 (branch AN1) with the antisymmetric state of u_{-1} (branch AN2). The branch D5 is linearly stable, while D6 is linearly unstable, as indicated in Fig. 4. Interestingly, the norm of these branches almost coincides with the norm of branches S0 (for D5) and AN0 (for D6) although they do not involve a nontrivial

component of u_0. This is apparently associated with the fact that branches such as D5 or D6 can be effectively described in the framework of SMA. On the other hand, clearly D1-D4 cannot; thus, they provide a distinct, potentially stable (and even symmetry-broken) set of states that could be accessible by the $F = 1$ spinor BEC system.
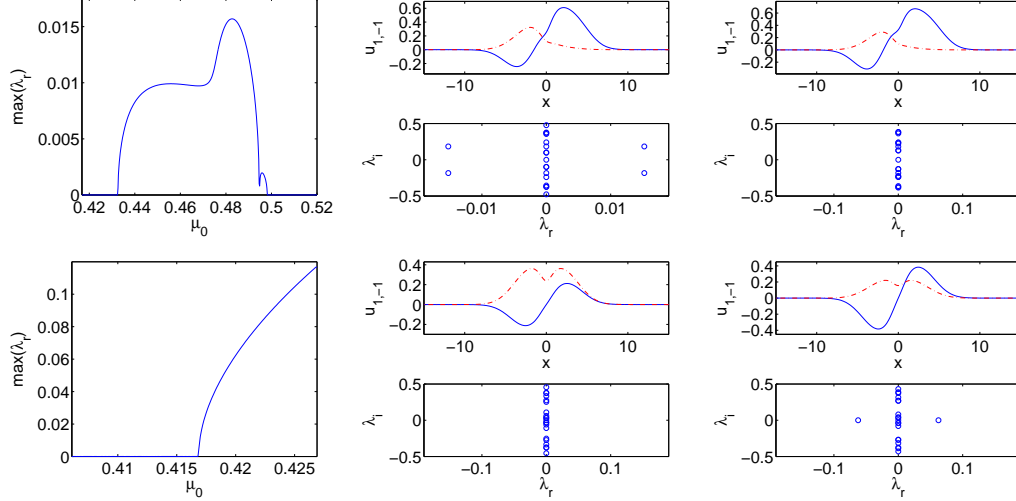

Figure 3: (Color online) Left panels: the maximum real eigenvalue as a function of μ_0 for D3 (top left) and D4 (bottom left) in Fig. 1. The middle and right panels show the profiles of wave functions (first and third row) u_1 and u_{-1} [by solid (blue) and dash-dotted (red) lines, respectively], together with the stability eigenvalues corresponding to D3 and D4: D3 for $\mu_0 = 0.48$ (top middle), D3 for $\mu_0 = 0.51$ (top right), D4 for $\mu_0 = 0.41$ (bottom middle) and D4 for $\mu_0 = 0.42$ (bottom right) with $\mu_{-1} = 0.38$ in the case of ^{23}Na condensate.
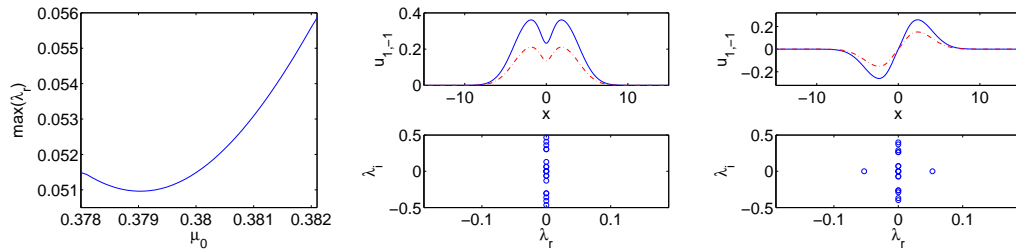

Figure 4: (Color online) The left panel shows the maximum real eigenvalue as a function of μ_0 for D6 in Fig. 1. The middle and right panels show the profiles of wave functions u_1 and u_{-1} by solid (blue) and dash-dotted (red) lines, respectively, together with stability eigenvalues corresponding to D5 and D6 in Fig. 1: D5 for $\mu_0 = 0.382$ (middle), D6 for $\mu_0 = 0.381$ (right).

3.2 Three-component states

We now turn to states involving all three components, such as the ones analyzed in Figs. 5 and 6. These branches resemble the ones that we analyzed above regarding states D1-D4; in particular, they connect S0 with AN1 (or with AN2) or AN0 with S1 (or with S2). However, there is a subtle

difference: in the case of the branches D1-D4 the coupling of the components u_1 and u_{-1} did not involve any contribution from (or to) component u_0, since in this case the last term in the system of Eqs. (2.1)-(2.2) is inactive. *However*, in the presence of a nonvanishing component u_0, this last (four-wave-mixing type) term becomes activated and even though the branch connects, say, S0 with AN1 (as is the case for the branch C2), this waveform introduces a contribution in the component u_{-1}, rendering the solution nonzero in all three components. Furthermore, the nature of the profile of u_0 and u_1 combined with the functional form of this term ($\propto u_0^2 u_1$) determine the parity of the u_{-1} component [in the case of C2 it should be anti-symmetric as is indeed shown in Fig. 5]. Out of this genuinely three-component solution C2, bifurcates an asymmetric variant thereof (again through a supercritical pitchfork) destabilizing the solution and the resulting new branch, C1, is asymmetric and again involves all three components of the spinor condensate. [It is worthwhile to note in passing that as shown in Fig. 5, the solution branch C2 could even be unstable prior to the critical point of the symmetry breaking pitchfork bifurcation due to a complex quartet and an associated oscillatory instability]. Branches C4 and C3 are the analogs of branches C2 and C1 but involve predominantly the component u_{-1} (and weakly generate the component u_1). Branches C3 and C1 eventually merge with AS2 and AS1 respectively. Then, branch C6 involves a similar coupling which joins S2 and AN0, as is shown in Fig. 1 and Fig. 6 (instead of S0 and AN2); out of that bifurcates the stable, three-component asymmetric branch C5 also shown in Fig. 6. The analog of C6 and C5 involving a coupling between components u_1 and u_0 (instead of u_{-1} and u_0) is given by the branches C8 and C7 which have also been identified in Fig. 1 (but for $\mu_{-1} = 0.48$). Branches C7 and C5 both merge with AS0 eventually. Notice that in the rightmost panel of the third row of Fig. 1, the branch C8 joining S1 and AN0 and the stable asymmetric branch C7 bifurcating off of that again appear to almost coincide (norm-wise). Importantly, it should be noted that none of these solutions can be captured in any way by the SMA.

On the other hand, as is evident in Fig. 1, by the comparison of the top right panel of the two-mode Galerkin-type approximation with the full results of the original system, the two-mode approximation performs very well in providing a semi-analytical prediction (obtained through the solution of a few simple nonlinear algebraic equations) of the bifurcation diagram of the full system. It is clear that quantitatively the two-mode approximation represents the relevant branches less accurately for higher values of the number of atoms N; e.g., the branch C1 reaches values of $N \approx 3$ as $\mu \to 0.52$ (at the right end of the Fig. 1), while from the two-mode approximation it only reaches $N \approx 2.5$. Nevertheless, the method traces in a systematic manner *all* the branches that can also be found in the full numerical results and their corresponding bifurcations.

From the above, it can be inferred that the full bifurcation diagram is extremely complex in the spinor BEC case involving not only "pure" one-component states, but also additional two-component and in fact even fully three-component "spinorial" states. The new emergent states are always a form of intermediary between original pure states and also possess symmetry breaking bifurcations of their own giving rise to genuinely spinorial, spatially symmetry broken states. Despite the fact that many of these states (including the asymmetric ones or even the symmetric/antisymmetric ones prior to their pitchfork bifurcation points) are genuinely stable dynamical states of the $F = 1$ spinor BEC system, they are *not* captured in the framework of the SMA.

Since Fig. 1 was constructed for a particular value of the chemical potential μ_{-1}, it is worth commenting on how the relevant features may change upon variation of μ_{-1}. For this reason, Fig.
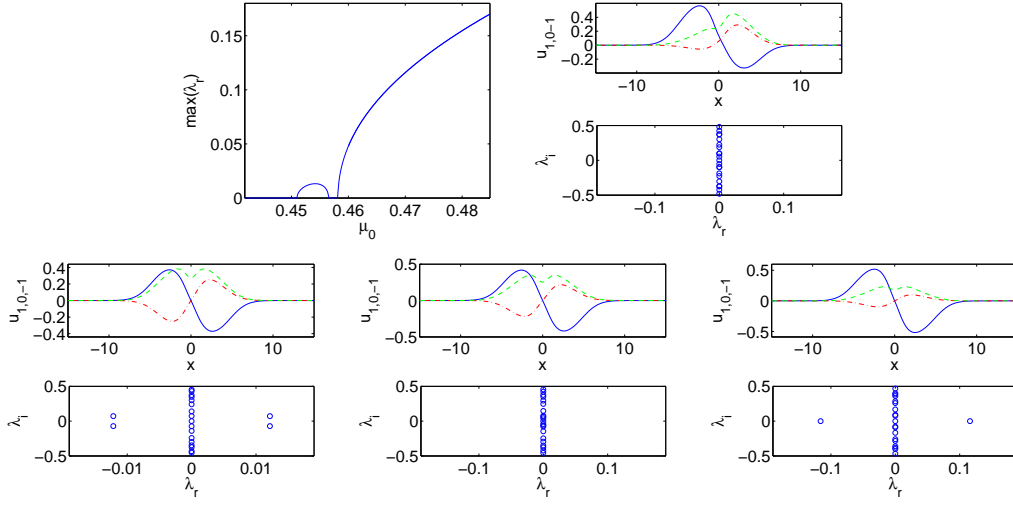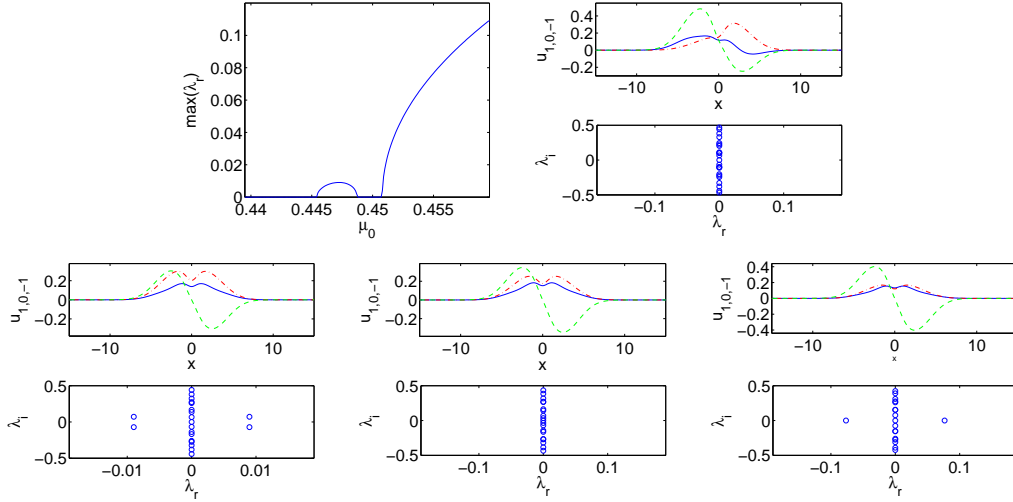
Figure 5: (Color online) The top left panel shows the maximum real eigenvalue as a function of μ_0 for C2 in Fig. 1. The other panels show the profiles of wave functions u_1, u_0 and u_{-1} by solid (blue), dashed (green) and dash-dotted (red) lines, respectively, and stability eigenvalues corresponding to branches C1 and C2 in Fig. 1: C1 for $\mu_0 = 0.48$ (top right), C2 for $\mu_0 = 0.453$ (bottom left), C2 for $\mu_0 = 0.457$ (bottom middle) and C2 for $\mu_0 = 0.47$ (bottom right) with $\mu_{-1} = 0.38$. The profiles of u_{-1} [dash-dotted (red) lines] are multiplied by 30 to be more visible.

Figure 6: (Color online) The top left panel shows the maximum real eigenvalue as a function of μ_0 for C6 in Fig. 1. The other panels show the profiles of wave functions u_1, u_0, u_{-1} [by solid (blue), dashed (green) and dash-dotted (red) lines, respectively], and stability eigenvalues corresponding to branches C5 and C6 in Fig. 1: C5 for $\mu_0 = 0.48$ (top right), C6 for $\mu_0 = 0.447$ (bottom left), C6 for $\mu_0 = 0.45$ (bottom middle) and C6 for $\mu_0 = 0.455$ (bottom right) with $\mu_{-1} = 0.38$. The profiles of u_1 [solid (blue) lines] are multiplied by 40 to be more visible.

11

7 examines both higher and lower values of this chemical potential (both in the full system, as well as in the reduced two-mode approximation of the six algebraic equations –left and right panels, respectively of the top two rows of the figure–). What is observed is that while a slight increase of the parameter does not substantially alter the phenomenology, a slight decrease thereof may result in a drastic decrease in the number of branches observed. This can be qualitatively understood as follows. When μ_{-1} is decreased, initially AS2, later AN2, and finally even S2 will disappear. For $\mu_{-1} = 0.28$ shown in Fig. 7, already branches AS2 and AN2 have disappeared and only S2 persists among the pure u_{-1} branches. As a result, all the branches that would "connect" to AN2 are also forced to disappear, including, e.g., D2 and D1, D3, D6 or C4, C3 and C5. Hence, as a rule of thumb, decreasing the chemical potentials (in this case of repulsive interactions) generally reduces the number of available states that can exist. A guide for potentially identifying such more complex combined states is the corresponding presence of "pure" states in the system. Notice that in all our considerations herein, we have focused on chemical potentials $\mu_{-1} < 0.61$ such that nonlinear modes associated with the second excited state do not become "activated". For higher values of the chemical potential, obviously such higher excited states will come into play and the two-mode Galerkin-type approximation will no longer be sufficient to address their existence. Nevertheless, in considering such higher excited states, we have typically observed them to be unstable and hence do not pursue them further herein.

We should note that we also considered along the same vein the bifurcation diagram for the case of the *ferromagnetic* ⁸⁷Rb spinor condensate (recall that in this case $\delta = \nu_a/\nu_s = -4.66 \times 10^{-3} < 0$). While this difference in the sign of δ plays a key role in important dynamical phenomena such as the modulational instability [37, 15, 19], nevertheless the structure and main features of the resulting state diagram are observed to essentially be the same between the two cases, perhaps due to the strong confinement considered here within the realm of the double well potential.

3.3 Dynamics

We now provide some representative examples of dynamics of the various branches. We commence by considering the branches D2, D4 and D6 respectively in the top, middle and bottom row of Fig. 8. We can see that the dynamics and instability of these branches does not strongly couple to the 0-th component of the spinorial state (and it only does because of the initial small amplitude noise seeded in that state, a seeding that takes place in all our simulations in the initial conditions). In that sense, the dynamical evolution of these states closely resembles the observations of Ref. [34]. In particular, we observe a nearly periodic breaking of the symmetry leading to amplification of one of the two components in one of the wells, while typically the other component is amplified in the other well [a notable exception to that is the case of D6 where the wavefunctions have the same parity, both being anti-symmetric].

Roughly similar behavior can be observed in the dynamics of the combined branches involving all three spinorial components, such as the ones for C2 and C8 in Fig. 9, as well as the ones for C4 and C6 in Fig. 10. In Fig. 9, the solution is predominantly supported in the components u_1 and u_0 (respectively u_{-1} and u_0 in Fig. 10) and has a small amplitude in the remaining component. The two predominant components exhibit similar recurrent behavior, whereby at roughly periodic intervals the solution becomes asymmetric with stronger support for one component in the one well,
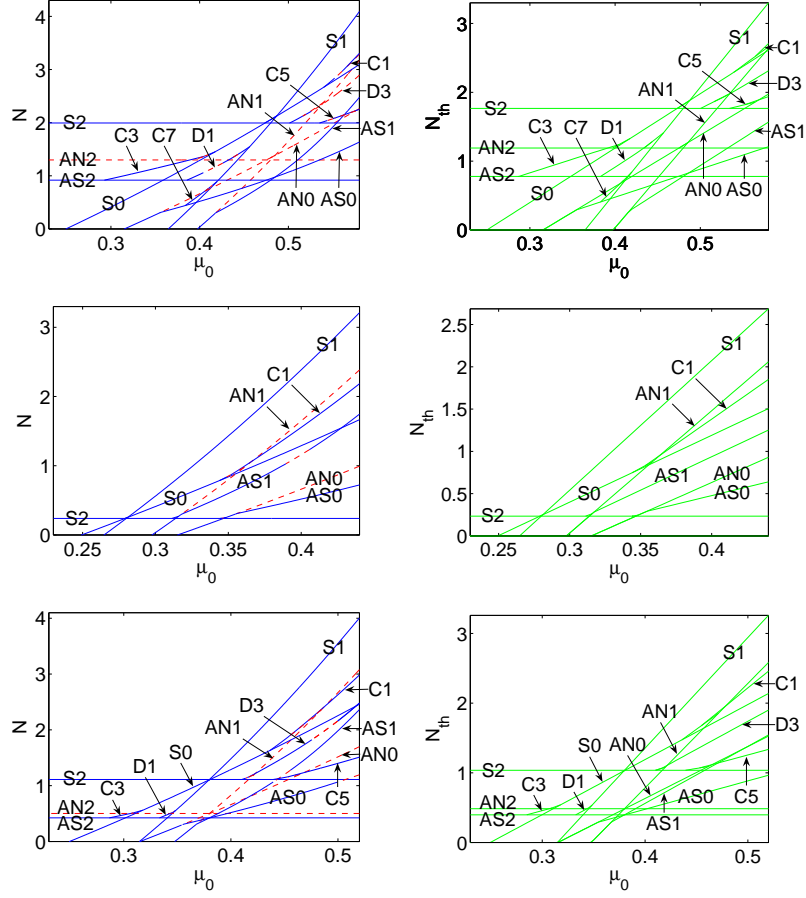
Figure 7: (Color online) The norm of the numerically found (left) and the approximate two-mode (right) solutions of Eqs. (2.1)-(2.2) as a function of μ_0 for $\mu_{-1} = 0.48$ (top) and $\mu_{-1} = 0.28$ (middle) in the case of ^{23}Na spinor BEC, and $\mu_{-1} = 0.38$ in the case of ^{87}Rb spinor BEC (bottom). The notation is the same as in Fig. 1.
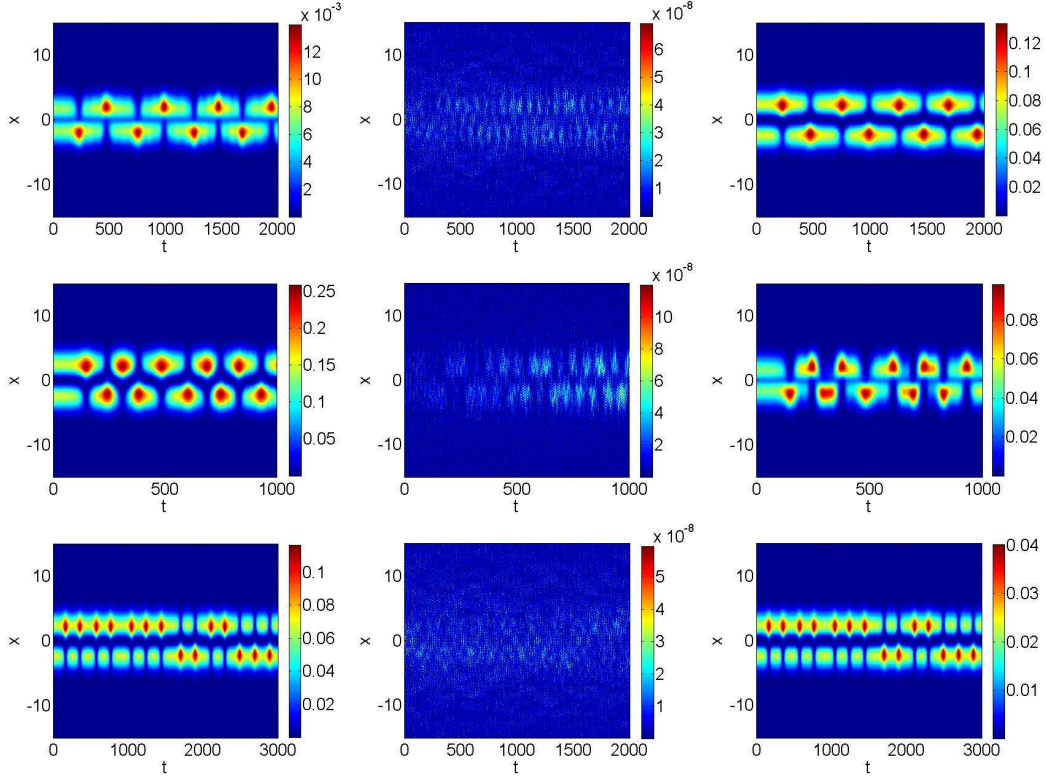
Figure 8: (Color online) Spatio-temporal contour plots of the densities of unstable combined two-component solutions in the case of ^{23}Na spinor BEC. The panels show the simulated evolution of wave functions ψ_1 (left), ψ_0 (middle) and ψ_{-1} (right) in unstable solutions of D2 (top), D4 (middle) and D6 (bottom) from Fig. 1, respectively.

while stronger support for the other component is in the second well. The weaker component is eventually more strongly amplified by the instability, but still does not appear to play a critical role in affecting the dynamics of the two dominant components. Nevertheless, we clearly see the symmetry-breaking manifestation of the relevant instability and the recurrent emergence of the ensuing asymmetric waveforms.
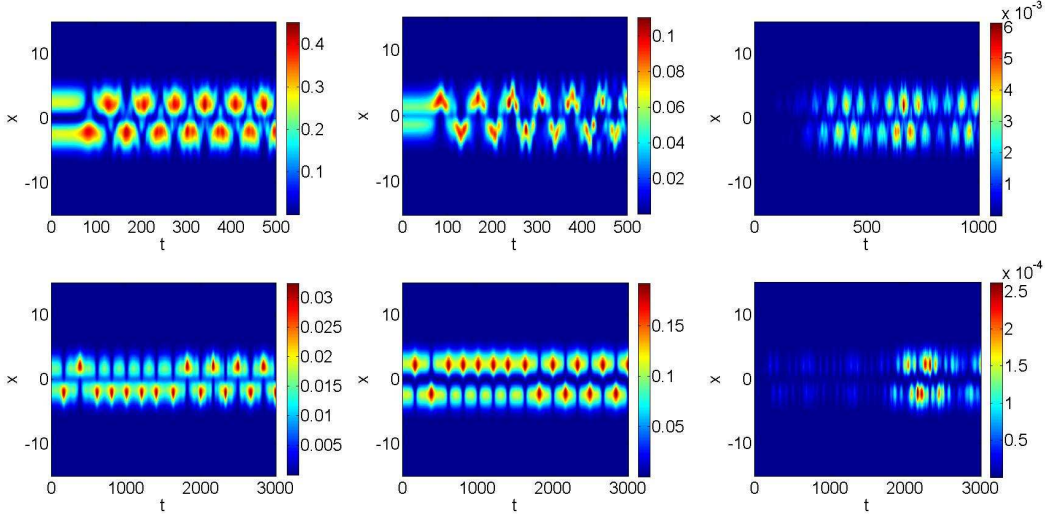

Figure 9: (Color online) Spatio-temporal contour plots of the densities, $|u_1|^2$, $|u_0|^2$ and $|u_{-1}|^2$, of unstable combined three-component solutions in the case of ^{23}Na spinor BEC. The top and bottom panels show the simulated evolution of wave functions ψ_1 (left), ψ_0 (middle) and ψ_{-1} (right) in unstable solutions of C2 (top) and C8 (bottom) from Fig. 1, respectively.
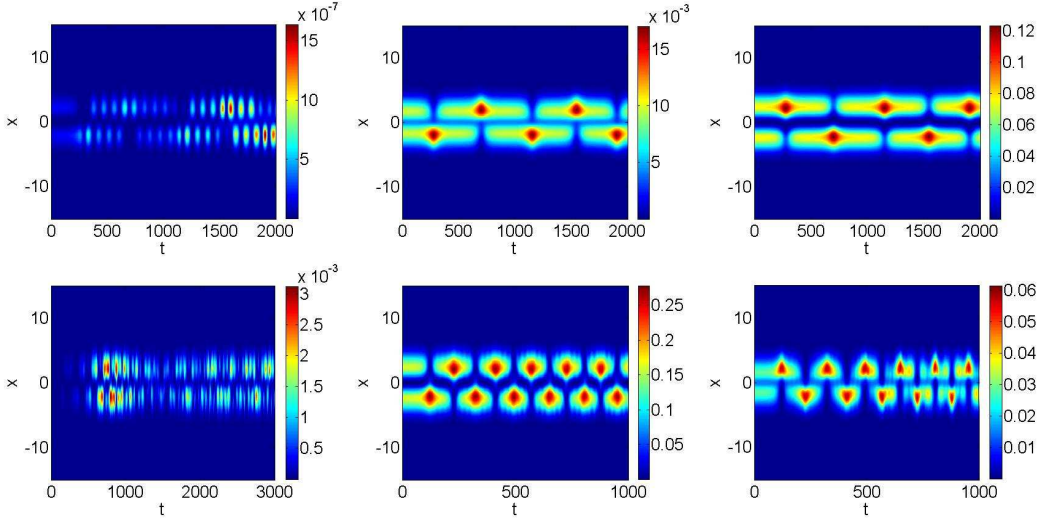

Figure 10: (Color online) Same as in Fig. 9. The top and bottom panels depict the simulated evolution of the densities of components 1 (left), 0 (middle) and -1 (right) in unstable solutions of C4 (top) and C6 (bottom) as shown in Fig. 1, respectively.

In all of the above examples, we have seeded the instability by a random (uniformly distributed)

15

perturbation imposed to the original stationary solutions with a small amplitude (10^{-4}), essentially emulating the presence of a background of experimental "noise" in a potential experiment. While this was not based on a physical model of quantum or thermal noise present in an actual experiment, the main thing that matters (at least in as far as the deterministic evolution of the mean field spinor models considered herein is concerned) is the projection of the relevant perturbation on the unstable eigendirection (i.e., eigenvector) of the linearization around the solution. Our results (for different amplitudes, as well as different realizations of the noise) clearly illustrate this fact (see below).

To illustrate the effect of the noise amplitude, we have repeated our numerical simulations with higher noise amplitudes (but with the same spatial distribution of the noisy perturbation); see Figs. 11 and 12. We can observe that in such a case the dynamics is principally similar [in all cases, the symmetry breaking still occurs, although its evolution in time may differ somewhat for different amplitudes cf. Fig.12]. The amplitude of the noise does play a role in the time scale of the manifestation of the instability, since the larger the initial noise amplitude, the shorter the time interval until it gets amplified (by the instability) to an O(1) perturbation.

Finally, to illustrate that the realizations of the noise (for the same noise amplitude) are not substantially different, we also did the following numerical experiment. We took ten different (spatial) realizations of the randomly distributed perturbation, but all of them with the same amplitude and then averaged the result. The relevant findings are presented in Fig. 13. The top panel of the figure shows the result of the average of the 10 random realizations of the perturbation (to be compared with the corresponding panel of Fig. 9). The difference between the two panels is shown in the bottom of Fig. 13, and is clearly minimal. Hence, for all ten realizations of essentially the same noise amplitude, the manifestation of the instability was essentially similar. This validates our claim above that the key element in this deterministic dynamical evolution is the projection of the perturbation to the dominant unstable eigenmode which dictates the dynamics of the instability development and its symmetry breaking manifestations.

Lastly, although, in the present work, we have used the two mode reduction as merely a tool for identifying the static solutions (and their bifurcations) for the full spinor system, let us briefly comment in passing about the dynamical properties of the two-mode model. Similarly to what has been suggested in [26], we find (results not shown here) that the dynamical results of the two-mode approximation are closer to the ones of the full GP equation for lower nonlinearities (i.e., closer to the linear limit) and higher potentials (i.e., a more pronounced double well structure).

4   Conclusions

In this work, we considered the statics and dynamics of a $F = 1$ spinor condensate confined in a double well potential. We illustrated that the two-mode Galerkin-type approximation, previously developed for one-component [28, 29] and two-component [34] settings can be extended to this genuinely three-component setting. The advantage of such a methodology is that it can offer considerable insight on the full set of stationary states that the system can exhibit, not only as pure states involving one-component, or two-component combinations (involving the ψ_1 and ψ_{-1} components), but even fully three-component spinorial states. An additional strength of the method is that it does not rely on the single mode approximation (SMA) that necessitates the same spatial
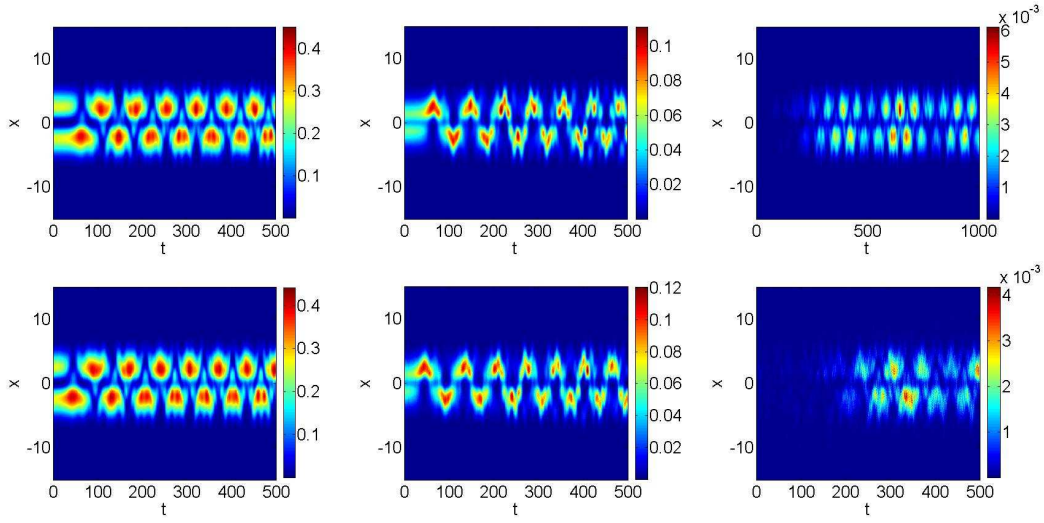
Figure 11: (Color online) Same as in Fig. 9. The top and bottom panels show the simulated evolution of the density of components 1 (left), 0 (middle) and -1 (right) in unstable solutions of C2. A random (uniformly distributed) noise of amplitude 10^{-3} (top) and 10^{-2} (bottom) is involved initially in perturbing the exact unstable solution, compared to the one of amplitude 10^{-4} in Fig. 9.
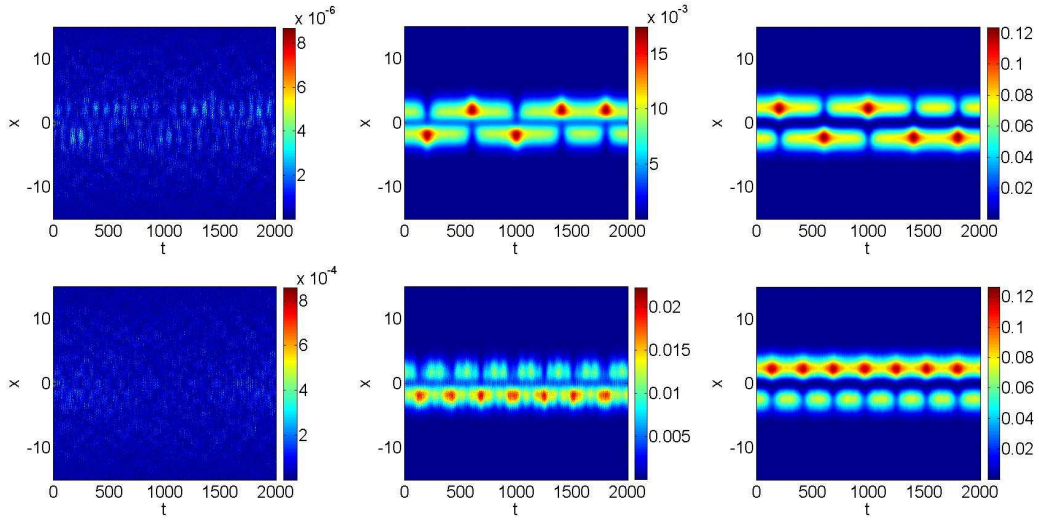

Figure 12: (Color online) Same as in Fig. 9. The top and bottom panels show the simulated evolution of components 1 (left), 0 (middle) and -1 (right) in unstable solutions of C4, with an initial random noise of amplitude 10^{-3} (top) and 10^{-2} (bottom), compared to the one of 10^{-4} in Fig. 10.
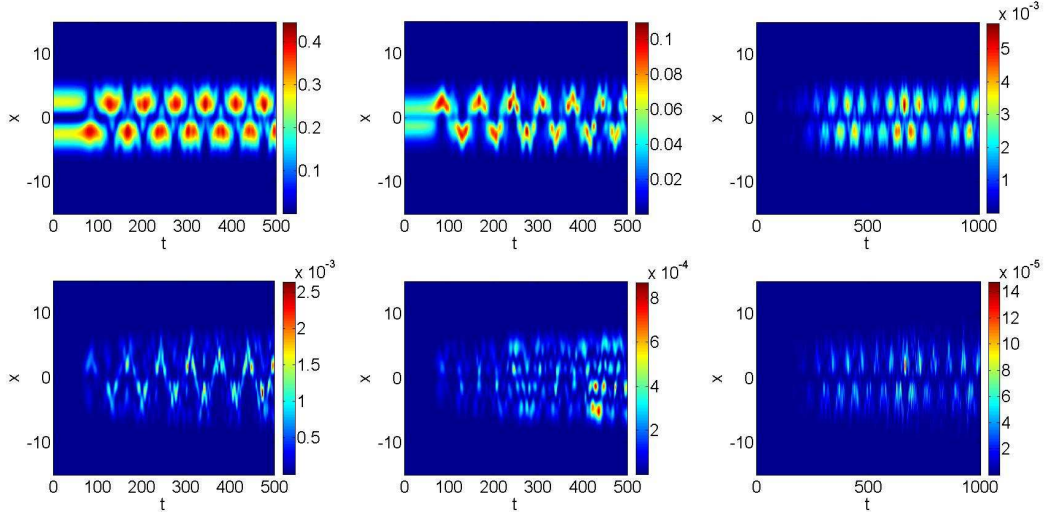
17

Figure 13: (Color online) Same as in Fig. 9. The top panels show the average of 10 simulated evolutions of the density of components 1 (left), 0 (middle) and −1 (right) in unstable solutions of C2 with different initial noises of amplitude 10^{-4}. The bottom panel is the difference between the top panels in this figure and the top panel in Fig. 9.

profile among all the hyperfine components, but rather it permits to fully explore non-SMA states that the system clearly and abundantly possesses. In fact, most of these states are observed to be dynamically stable in at least a fraction of parameter space of their existence (i.e., effectively for appropriate atom numbers) and hence should be accessible to relevant experiments with spinor condensates in double well potentials. We have observed that the two-mode Galerkin-type approximation is very efficient in unraveling the full bifurcation diagram of the possible states. Finally, we have illustrated the dynamics of either two-component or three-component spinorial states in direct simulations, observing typically the emergence of the symmetry breaking instability, leading to a stronger population of one or the other well, and subsequent recurrence of such asymmetric patterns.

There are many directions that open up with respect to this analytical description of the double well system. On the one hand, one can extend this two-mode Galerkin-type approximation to a higher-number of mode description (that, for instance, will involve higher excited states) so that one can describe the possible situations for higher numbers of atoms/chemical potentials. On the other hand, one can extend the present theory to the mean-field description of a $F = 2$ spinor condensate following, e.g., the description of [43] (see also references therein). Finally, yet another interesting direction (even for the $F = 1$ case) is to extend the present considerations to the simplest higher-dimensional case, involving four wells arranged along the nodes of a square and attempting a corresponding four-mode reduction for each of the components. In that setting, it would be especially interesting to identify multi-pole structures and topological states, such as vortices, among others. Such studies are currently in progress and will be reported elsewhere.

18

A   Special Case Examples of Solutions

In this Appendix we consider some special cases, in which the solutions of the algebraic equations of our two-mode reduction are analytically tractable (or, in any case, reduce to previously addressed problems with a lower number of components). More specifically, there exist *one-component* states which can be found in the case where, e.g., $c_{a,b}^{(\pm 1)} = 0$. In this case, we can readily identify a purely *symmetric* state with

$$(c_a^{(0)})^2 = \frac{\mu_0 - \omega_a}{\nu_s \Gamma_a}, \quad c_b^{(0)} = 0, \tag{A.1}$$

as well as a purely *anti-symmetric* state with

$$c_a^{(0)} = 0, \quad (c_b^{(0)})^2 = \frac{\mu_0 - \omega_b}{\nu_s \Gamma_b}. \tag{A.2}$$

Finally, there is also a mixed or *asymmetric* state with

$$(c_a^{(0)})^2 = \frac{(\mu_0 - \omega_a)\Gamma_b - 3(\mu_0 - \omega_b)\Gamma_{ab}}{\nu_s(\Gamma_a\Gamma_b - 9\Gamma_{ab}^2)}, \quad (c_b^{(0)})^2 = \frac{(\mu_0 - \omega_b)\Gamma_a - 3(\mu_0 - \omega_a)\Gamma_{ab}}{\nu_s(\Gamma_a\Gamma_a - 9\Gamma_{ab}^2)}. \tag{A.3}$$

The mixed branch bifurcates beyond a critical value of μ_0 from the symmetric state if $\nu_s < 0$, or from the antisymmetric state if $\nu_s > 0$ [29]. It is important to note here that such pure and mixed states exist also in components ± 1, with the only difference in their definition (except for the $0 \to \pm 1$ in the indices above) that $\nu_s \to \nu_s + \nu_a$.

In addition to the above setting, there is another case where these pure and mixed mode states appear (now in all three components), namely in the spinor BEC description in the framework of SMA [11, 37, 38] (see also discussion in [18]). In that case, $\mu_0 = \mu_1 = \mu_{-1} = \mu$ and $u_j = s_j u(x)$, where u satisfies the single component equation

$$\mu u = \mathcal{L}u + \nu_s u^3, \tag{A.4}$$

while the coefficients s_j containing the spin degree of freedom are given by,

$$s_1 = \cos^2(\frac{\beta}{2}), \quad s_0 = \sqrt{2}\cos(\frac{\beta}{2})\sin(\frac{\beta}{2}), \quad s_{-1} = \sin^2(\frac{\beta}{2}) \tag{A.5}$$

$$s_1 = -\frac{1}{\sqrt{2}}\sin(\beta), \quad s_0 = \cos(\beta), \quad s_{-1} = \frac{1}{\sqrt{2}}\sin(\beta), \tag{A.6}$$

where β is a free parameter. In the context of SMA, which is generally valid if the condensate width is far smaller than the spin healing length (so that the terms proportional to ν_a do not substantially influence the dynamics), again the possible solutions reduce to the above pure and mixed modes.

Finally, yet another special case is the one corresponding to the existence of *two-component* states. In paricular, in the case $u_0 = 0$, the three-component system degenerates to the two-component setting recently considered in [34], with self-phase modulation proportional to $\nu_s + \nu_a$ and cross-phase modulation proportional to $\nu_s - \nu_a$. Based on the analysis of [34], two-component states, both symmetric and antisymmetric, but also mixed two-component states are expected to exist.

References

[1] C. J. Pethick and H. Smith, *Bose-Einstein condensation in dilute gases*, Cambridge University Press (Cambridge, 2002).

[2] L. P. Pitaevskii and S. Stringari, *Bose-Einstein Condensation*, Oxford University Press (Oxford, 2003).

[3] P. G. Kevrekidis, D. J. Frantzeskakis, and R. Carretero-González (eds.), *Emergent nonlinear phenomena in Bose-Einstein condensates. Theory and experiment* (Springer-Verlag, Berlin, 2008).

[4] Yu. S. Kivshar and G. P. Agrawal, *Optical Solitons: From Fibers to Photonic Crystals*, (Academic Press, San Diego, 2003).

[5] D. M. Stamper-Kurn and W. Ketterle, cond-mat/0005001.

[6] D. M. Stamper-Kurn, M. R. Andrews, A. P. Chikkatur, S. Inouye, H.-J. Miesner, J. Stenger, and W. Ketterle, Phys. Rev. Lett. **80**, 2027 (1998).

[7] M.-S. Chang, C. D. Hamley, M. D. Barrett, J. A. Sauer, K. M. Fortier, W. Zhang, L. You, and M. S. Chapman, Phys. Rev. Lett. **92**, 140403 (2004).

[8] J. Kronjäger, C. Becker, M. Brinkmann, R. Walser, P. Navez, K. Bongs, and K. Sengstock, Phys. Rev. A **72**, 063619 (2005).

[9] J. Stenger, S. Inouye, D. M. Stamper-Kurn, H.-J. Miesner, A. P. Chikkatur, and W. Ketterle, Nature (London) **396**, 345 (1998).

[10] A. E. Leanhardt, Y. Shin, D. Kielpinski, D. E. Pritchard, and W. Ketterle, Phys. Rev. Lett. **90**, 140403 (2003).

[11] H. Pu, C.K. Law, S. Raghavan, J.H. Eberly, and N.P. Bigelow, Phys. Rev. A **60**, 1463 (1999).

[12] S. Yi, Ö. E. Müstecaplioglu, and L. You, Phys. Rev. A **68**, 013613 (2003).

[13] Ö. E. Müstecaplioglu, M. Zhang, S. Yi, L. You, and C.P. Sun, Phys. Rev. A **68**, 063616 (2003).

[14] J. Ieda, T. Miyakawa, and M. Wadati, Phys. Rev. Lett. **93**, 194102 (2004); J. Phys. Soc. Jpn. **73**, 2996 (2004).

[15] L. Li, Z. Li, B. A. Malomed, D. Mihalache, and W. M. Liu, Phys. Rev. A **72**, 033611 (2005).

[16] W. Zhang, Ö. E. Müstecaplioglu, and L. You, Phys. Rev. A **75**, 043601 (2007).

[17] M. Uchiyama, J. Ieda, and M. Wadati, J. Phys. Soc. Jpn. **75**, 064002 (2006).

[18] B.J. Dabrowska-Wüster, E.A. Ostrovskaya, T.J. Alexander and Yu.S. Kivshar, Phys. Rev. A **75**, 032617 (2007).

[19] H. E. Nistazakis, D. J. Frantzeskakis, P. G. Kevrekidis, B. A. Malomed, and R. Carretero-González, Phys. Rev. A **77**, 033612 (2007).

[20] H. E. Nistazakis, D. J. Frantzeskakis, P. G. Kevrekidis, B. A. Malomed, R. Carretero-González, and A. R. Bishop, Phys. Rev. A **76**, 063603 (2007).

[21] M. Albiez, R. Gati, J. Fölling, S. Hunsmann, M. Cristiani, and M. K. Oberthaler, Phys. Rev. Lett. **95**, 010402 (2005).

[22] S. Raghavan, A. Smerzi, S. Fantoni, and S. R. Shenoy, Phys. Rev. A **59**, 620 (1999); S. Raghavan, A. Smerzi and V. M. Kenkre, Phys. Rev. A **60**, R1787 (1999); A. Smerzi and S. Raghavan, Phys. Rev. A **61**, 063601 (2000).

[23] E. A. Ostrovskaya, Y. S. Kivshar, M. Lisak, B. Hall, F. Cattani, and D. Anderson, Phys. Rev. A **61**, 031601 (R) (2000).

[24] K. W. Mahmud, J. N. Kutz and W. P. Reinhardt, Phys. Rev. A **66**, 063607 (2002).

[25] V. S. Shchesnovich, B.A. Malomed, and R. A. Kraenkel, Physica D **188**, 213 (2004).

[26] D. Ananikian, and T. Bergeman, Phys. Rev. A **73**, 013604 (2006).

[27] P. Ziń, E. Infeld, M. Matuszewski, G. Rowlands, and M. Trippenbach, Phys. Rev. A **73**, 022105 (2006).

[28] T. Kapitula and P. G. Kevrekidis, Nonlinearity **18**, 2491 (2005).

[29] G. Theocharis, P.G. Kevrekidis, D.J. Frantzeskakis and P. Schmelcher, Phys. Rev. E **74**, 056608 (2006).

[30] D. R. Dounas-Frazer and L .D. Carr, arXiv:quant-ph/0610166.

[31] C. Cambournac, T. Sylvestre, H. Maillotte, B. Vanderlinden, P. Kockaert, Ph. Emplit, and M. Haelterman, Phys. Rev. Lett. **89**, 083901 (2002).

[32] P. G. Kevrekidis, Z. Chen, B. A. Malomed, D. J. Frantzeskakis, and M. I. Weinstein, Phys. Lett. A **340**, 275 (2005).

[33] E.B. Becker, G.F. Carey and T.J. Oden, *Finite Elements: An Introduction*, Prentice-Hall (Englewood Cliffs, 1981).

[34] C. Wang, P.G. Kevrekidis, N. Whitaker, and B.A. Malomed, arXiv:0805.0023; Physica D, in press (2008).

[35] Ö.E. Müstecaplioglu, W. Zhang and L. You, Phzs. Rev. A **71**, 053616 (2005).

[36] Ö.E. Müstecaplioglu, W. Zhang and L. You, Phzs. Rev. A **75**, 023605 (2007).

[37] N. P. Robins, W. Zhang, E. A. Ostrovskaya, and Y. S. Kivshar, Phys. Rev. A **64**, 021601(R) (2001).

[38] S. Yi, Ö. E. Müstecaplioglu, C. P. Sun, and L. You, Phys. Rev. A **66**, 011601(R) (2002).

[39] P.B. Lundquist, D.R. Andersen and Yu.S. Kivshar, Phys. Rev. E **57**, 3551 (1998).

[40] E. G. M. van Kempen, S. J. J. M. F. Kokkelmans, D. J. Heinzen, and B. J. Verhaar, Phys. Rev. Lett. **88**, 093201 (2002).

[41] N. N. Klausen, J. L. Bohn, and C. H. Greene, Phys. Rev. A **64**, 053602 (2001).

[42] J.-C. van der Meer, Nonlinearity **3**, 1041 (1990).

[43] H. Saito and M. Ueda, Phys. Rev. A **72**, 053628 (2005).